

Joint 3rd UK-China Steel Research Forum & 15th CMA-UK Conference on Materials Science and Engineering

## Self-consistent modelling and the evaluation of lattice deformation in a polycrystalline austenitic stainless steel

Jianan Hu<sup>1,\*</sup>, Bo Chen<sup>2</sup>, David J. Smith<sup>3</sup>, Peter E.J. Flewitt<sup>4</sup>, Alan C.F. Cocks<sup>1</sup>

<sup>1</sup>*Department of Engineering Science, University of Oxford, Oxford, OX1 3PJ, UK*

<sup>2</sup>*Materials Performance Centre, School of Materials, University of Manchester, M13 9PL, UK*

<sup>3</sup>*Department of Mechanical Engineering, University of Bristol, BS8 1TR, UK*

<sup>4</sup>*H.H. Wills Physics Laboratory, University of Bristol, BS8 1TL, UK*

---

### Abstract

Individual anisotropic grains within a polycrystalline material exhibit different micro-mechanical responses for a given applied macroscopic stress, leading to a variation in the meso-scale intragranular lattice strain. Despite various experimental data for the lattice strain evolution measured by neutron diffraction, a physical understanding of how the lattice strain evolves during plastic flow is still incomplete. In this study, a self-consistent model is established, taking into account detailed dislocation kinetics and its influence on different evolution processes of the dislocation distribution on different crystallographic planes of each grain within a polycrystalline material. The model is used to evaluate the micro-mechanical behaviour of F.C.C. polycrystalline austenitic stainless steels. Predictions of the lattice strain developed within individual grains of a polycrystal are compared with experimental results obtained using neutron diffraction. This model captures the major trends in the evolution of the lattice strains and provides an explanation and interpretation of the internal processes that most influence the observed response.

© 2015 The Authors. Published by Elsevier Ltd. This is an open access article under the CC BY-NC-ND license (<http://creativecommons.org/licenses/by-nc-nd/4.0/>).

Selection and Peer-review under responsibility of the Chinese Materials Association in the UK (CMA-UK).

**Keywords:** Self-consistent model; Austenitic stainless steel; Lattice deformation; Neutron diffraction

---

---

\* Corresponding author. Tel.: +44 (0)1865 283496.

E-mail address: [jianan.hu@eng.ox.ac.uk](mailto:jianan.hu@eng.ox.ac.uk)

## 1. Introduction

Polycrystalline austenitic stainless steels have a F.C.C structure. Elastic and plastic anisotropy of the individual grains within the polycrystal gives rise to variations in the micro-mechanical lattice response of differently oriented grains when it is subjected to an applied load. Intragranular residual stresses develop due to the plastic mismatch between grains, which may be detrimental to the macroscopic material performance [1, 2]. Therefore, understanding the micro-mechanical variation between differently orientated grains is vital to assessing the materials performance.

The non-destructive neutron diffraction technique has been used recently to measure the *in situ* evolution of micro-scale elastic lattice strains and residual elastic lattice strains for different subsets of grains within the bulk of polycrystalline austenitic stainless steels during macroscopic deformation [1-5]. Many constitutive models (e.g. self-consistent models) and/or finite element analyses have been used to simulate the relationship between the behaviour of the individual grains and that of the polycrystalline aggregate to predict the micro-scale behaviour of such materials [1, 2, 5]. Some of these studies have also incorporated a simplified dislocation slip mechanism to elaborate the hardening behaviour [1, 5]. However, none of these works have linked the work hardening observed macroscopically to the detailed evolution of dislocation structure associated with slip processes in each grain of the polycrystal. In addition, to date, no systematic study has compared the models of this type with micro-scale measurements to identify the dominant lattice deformation mechanisms.

In the present study, an improved multi-scale self-consistent polycrystal model is established, taking into account the detailed evolution of the dislocation distribution on different crystallographic planes of individual grains, the associated hardening mechanism and its influence on the micro-scale lattice deformation. This work is an extension of a previous study [6]. The model is used to predict and evaluate the micro-scale lattice response of a typical subset of grains within a Type 316H austenitic stainless steel under uniaxial tensile loading at ambient temperature. Various sources of *in situ* neutron diffraction measurements of this subset, both along the longitudinal (axial) and transverse (radial) directions with regard to the loading direction are compared and illustrated.

## 2. Self-consistent model for polycrystal

The self-consistent model consists of three parts, continuum, crystal plasticity and dislocation link length models, with the last of these based on a model originally proposed by Lagneborg and co-workers [7, 8]. The first two parts have been presented previously [6] and will only be briefly described here. The principal concern of this paper is the slip kinetics and the microstructure evolution of each individual grain, which will be described in detail later.

### 2.1. Continuum model of individual grains and polycrystal

The continuum model utilizes solutions of the classical Eshelby inclusion problem [9, 10]. The self-consistent scheme [6] establishes the elastic relationship between each individual inhomogeneous or anisotropic grain response and the polycrystalline aggregate response by an equivalent homogeneous inclusion with a properly chosen stress-free misfit strain. Given a macroscopically applied stress  $\sigma$ , the response of each individual grain is given by [6]

$$\varepsilon^{ia} + \left[ (C^a)^{-1} - (C^i)^{-1} \right] T \sigma = \left[ (C^a)^{-1} C^i (I - S^i) + S^i \right] \varepsilon^{is*} \quad (1)$$

where  $C^a, C^i$  are respectively the elastic stiffness matrices for the inhomogeneous grain and the isotropic polycrystal;  $S^i$  is the Eshelby tensor, related to the geometry of the grain and Poisson's ratio of the isotropic polycrystal [9, 10];  $\varepsilon^{ia}$  and  $\varepsilon^{is*}$  are respectively the misfit strain in the inhomogeneous grain and the equivalent homogeneous inclusion;  $T$  is the orientation matrix for the grain described by the angles that the outward normal to the faces of the cubic unit cell of the local F.C.C grain make with the axes of the global co-ordinate system and  $I$  is the unity matrix. Physically the misfit strain  $\varepsilon^{ia}$  is due to plastic deformation of the grain. Therefore, during elastic deformation  $\varepsilon^{ia} = 0$ , and  $\varepsilon^{is*}$  can be solved as a function of  $\sigma$ , allowing the stress and strain in each grain to be determined with respect to a local co-ordinate system co-incident with the outward normal to the faces of the unit cell:

$$\sigma^a = \left\{ \left[ \left[ I - (S^i)^{-1} \right]^{-1} (C^i)^{-1} - (C^a)^{-1} \right]^{-1} \left[ (C^a)^{-1} - (C^i)^{-1} \right] + I \right\} T \sigma = H^a T \sigma \quad (2a)$$

$$\varepsilon^a = \left\{ (C^i)^{-1} + \left[ \left[ (C^a)^{-1} - (C^i)^{-1} \right]^{-1} (C^a)^{-1} C^i (S^i)^{-1} - C^i \right]^{-1} \right\} T \sigma = K^a T \sigma \quad (2b)$$

where  $H^a$  and  $K^a$  are the quantities in the braces. During plastic deformation, incompatible plastic strains accumulate in each grain, i.e.  $\varepsilon^{ta} \neq 0$ . Kroner, Budiansky and Wu [11, 12] have expressed the mismatch between each grain and the surrounding matrix as (shown in an incremental form here)

$$\Delta \varepsilon^{ta} = \Delta \varepsilon^p - T^{-T} \Delta E^p \quad (3)$$

where  $\Delta \varepsilon^p$  is the plastic strain increment in the grain with respect to the local co-ordinate system and  $\Delta E^p$  is the macroscopic plastic strain increment of the bulk with respect to the global co-ordinate system, which can be determined from the plastic strain increments in all the grains of the bulk by the virtual work principle [13]. The  $T^{-T}$  used in Eq. (3) is due to the transformation between the mathematical strain component and the engineering strain component.  $\varepsilon^{ts}$  in Eq. (1) can be solved only explicitly as a function of  $\varepsilon^{ta}$  during macroscopic unloading ( $\sigma = 0$ ) and is then used to derive the change of the intragranular residual stress and elastic strain field ( $\Delta X^a, \Delta \varepsilon_r^e$ )

$$\Delta X^a = C^i (I - S^i) \left( (C^a)^{-1} C^i S^i - (C^a)^{-1} C^i - S^i \right)^{-1} \Delta \varepsilon^{ta} \quad (4a)$$

$$\Delta \varepsilon_r^e = (C^a)^{-1} \Delta X^a \quad (4b)$$

where these are defined in the local co-ordinate system. Finally, the total stress in each grain during plasticity is obtained as the combined contribution from the applied stress and the accumulation of residual stress at each step.

$$\Delta \sigma^a = H^a T \Delta \sigma + \Delta X^a \quad (5)$$

## 2.2. Crystal plasticity model for individual grains

The crystal plasticity model provides the plastic strain increment,  $\Delta \varepsilon^p$ , of each grain within the bulk to feed into the continuum model. Each F.C.C. grain contains four slip planes and each plane has three slip directions, giving totally twelve slip systems. If  $\bar{n}^\beta$  is the normal to a plane and  $\bar{s}^\beta$  is one of the slip directions associated with the slip system  $\beta$ ,  $\Delta \varepsilon^p$  is obtained by adding all the shear strain increments  $\Delta \gamma^\beta$  on all the active slip systems [14, 15]

$$\Delta \varepsilon^p = \sum_{\beta}^{12} \text{sym}(\Delta \gamma^\beta \bar{n}^\beta \otimes \bar{s}^\beta) = \sum_{\beta}^{12} \theta^\beta \Delta \gamma^\beta = \sum_{\beta}^{12} \theta^\beta \cdot \Delta \gamma_0 \left| \frac{\tau^\beta}{\tau_{cr}^\beta} \right|^p \text{sgn}(\tau^\beta) \quad (6)$$

where  $\theta^\beta = \text{sym}(\bar{n}^\beta \otimes \bar{s}^\beta)$  is the Schmid factor of the slip system  $\beta$  and  $\otimes$  represents the dyadic product. A power-law relationship [14, 16] is employed on the right hand side of Eq. (6), between the strain increment  $\Delta \gamma^\beta$  associated with the slip system  $\beta$  and the resolved shear stress (RSS)  $\tau^\beta$  as well as the critical resolved shear stress (CRSS)  $\tau_{cr}^\beta$  on that system, within a prescribed time step  $\Delta t$ .  $p$  is a rate sensitivity exponent and  $\Delta \gamma_0 = \dot{\gamma}_0 \Delta t$  is a reference shear strain increment. A large value of  $p$  is used to simulate rate-independent behaviour. Since the plastic shear strain is generated by the dislocation slip, this indicates that slip only occurs on  $\beta$  when  $\tau^\beta$  is approximately equal to  $\tau_{cr}^\beta$ . Use of a rate-independent model facilitates the automatic selection of the active slip systems at each time step. In addition,  $\tau^\beta$  is also related to the grain stress  $\sigma^a$  through the Schmid factor  $\theta^\beta$ :

$$\tau^\beta = \theta^\beta \sigma^a \quad (7)$$

Eqs. (5) and (7) can then be used to update the RSS at each step. Furthermore, for F.C.C. crystals, it is understood that the coplanar slip systems belonging to the same slip plane have identical CRSS [17], thus the hardening effect associated with the dislocation slip can be simplified based on slip planes rather than on slip systems.

### 2.3. Athermal dislocation link length model for individual slip planes

#### 2.3.1 Distribution of link lengths

This part of model employs a concept originally developed by Lagneborg and co-workers [7, 8], which describes the dislocation structure as a three-dimensional network of dislocation links with various lengths. Here a dislocation link is defined as the dislocation segment between two pinning points. In the present model, the pinning points on a slip plane refer to only the dislocation junctions, which are the intersections of links from other slip planes. Within this network, all the links are initially pinned by two points while each point also connects two links; thus the link length distribution is related to the distribution of pinning points. To describe the evolution of the dislocation structure on each elementary slip plane, a two-dimensional distribution function was established using a statistical analysis by Hu et al [13], which is associated with a random distribution of pinning points.

Given a slip plane with  $N$  randomly distributed pinning points per unit area, we assume that a link connects each point to its nearest neighbour. The two-dimensional distribution function  $\phi(\lambda)$  can then be written as [13]

$$\phi(\lambda) = \frac{2\pi\lambda}{L^4} \exp\left(-\frac{\pi\lambda^2}{L^2}\right) \quad (8)$$

where  $\phi(\lambda) \cdot \Delta\lambda$  equals the number of pinning points per unit area with the spacing in the range  $\lambda$  to  $\lambda + \Delta\lambda$ , or the number of potential links per unit area with lengths in the same range.  $L = N^{-1/2}$  is the mean spacing of all the pinning points on the slip plane, which is equivalent to the dislocation mean free path described in the literature [18-24]. A shear resistance to the connected link exerted by the pinning points is inversely proportional to the length [7]

$$\lambda = \frac{\alpha Gb}{\tau} \quad (9)$$

where  $\alpha$  is a constant determining the strength of the pinning points [25, 26], with an estimated value  $\alpha \approx 0.35$  for dislocation junctions [27].  $G$  is the shear modulus of a single grain and  $b$  is the Burgers vector. In an athermal problem, the link can be released from the pinning points and glide or expand only when the resolved shear stress approaches the shear resistance. In terms of Eq. (9), the resolved shear stress which initiates the plastic flow on a slip plane is associated with a limited or threshold link length  $\lambda_{th}$ . The presence of threshold links indicates that the spectrum of the link lengths on the slip plane should be in the range 0 to  $\lambda_{th}$ , not to infinity which has been considered in all the previous works [22]. Therefore, within the distribution of pinning points described by Eq. (8), only the points with spacing less than  $\lambda_{th}$  are connected with links, while links longer than  $\lambda_{th}$  cannot occur, i.e. the distribution of link lengths is a truncation of the distribution of pinning points.

It is reasonable to assume that all the slip planes within the single crystal have an initially identical distribution of pinning points and dislocation link length given by Eq. (8). However, as the crystal deforms, the evolution of dislocation distribution on different slip planes may vary.

#### 2.3.2 Dislocation kinetic motion

Lagneborg and Forsen [7] have described dislocation motion in terms of long waiting times at the obstacles and occasional spurt-like movements of links between obstacles. Therefore, all the dislocation links in the network can

be considered as held up at obstacles at any instant. Once the RSS increases and activates the threshold links, free glide motion occurs. These mobile links bypass obstacles and sweep out an area before being partitioned into shorter links by other obstacles (either pre-existing or newly created) and become immobile again. Then the RSS needs to increase further to mobilize the updated threshold links and continue the glide motion. If the area swept out by each mobile link is  $s$ , the generated shear strain increment  $\Delta\gamma$  on the slip plane by all the mobile links is expressed as

$$\Delta\gamma = s\Delta N_m = s\phi_{th} |\Delta\lambda_{th}| \quad (10)$$

where  $\Delta N_m = \phi_{th} |\Delta\lambda_{th}|$  is the number of mobilized threshold links per unit area and  $\phi_{th} = \phi(\lambda_{th})$  is the threshold value of the distribution function. The sign of  $\Delta\gamma$  depends on the slip direction. According to Foreman and Makin [25], the CRSS of the slip plane can be defined as the shear stress for dislocations to penetrate the whole slip plane and is inversely proportional to the mean spacing defined previously

$$L = \frac{\alpha Gb}{\tau_{cr}} \quad (11)$$

At this condition, the sweeping area  $s$  and the shear strain increment  $\Delta\gamma$  in Eq. (10) would become infinity. This feature of the plastic flow can be captured by assigning a large value to  $\Delta\gamma_0$  in Eq. (6), thus when the value of the RSS  $\tau$  (the largest among the coplanar systems) is equal to the CRSS  $\tau_{cr}$  on that slip plane, a large shear strain increment would be generated. By this treatment, the detailed derivation of the sweeping area on the slip plane is not needed since it can be automatically calculated by Eq. (6) and Eq. (10). It should be noted that  $\Delta\gamma$  on a slip plane is the sum of the shear strain increments on all the active coplanar slip systems on the corresponding plane.

### 2.3.3 Hardening with dislocation multiplication

As the dislocations glide along a slip plane, they interact with each other and multiply, creating new junctions, leading to the redistribution of the pinning points or equivalent, the dislocation links. The addition of new junctions hardens the slip plane by reducing the mean spacing thus increasing the CRSS  $\tau_{cr}$  according to Eq. (11). The multiplication process generally consists of three stages: multiple release of links; glide or expansion and mutual partitioning, with this last stage named network refinement [20]. Hardening on a slip plane by the increase of pinning points on the same plane is called self-hardening, which is associated with all the three stages, while that by multiplication on other intersecting planes is called latent hardening, and involves only network refinement. The original model [7, 8] seems to assume all the slip planes experience identical hardening. Here a simple statistical framework is developed to distinguish self- and latent hardening. We focus first on the case with only one active slip plane, while cases with multiple active slip planes can be simply analysed by superposition.

#### 2.3.3.1 Network refinement

Network refinement refers to mutual partitioning between the mobilized links on a slip plane and links on other slip planes. This process produces links shorter than the threshold links, which become new members of the network. If each mobilized link cuts  $j$  intersecting links on average at each step, the total number of cut per unit area would be  $j\Delta N_m$ . Each cut results in the destruction of two links with the formation of four new links, thus the increase in the total number of links in the network is simply  $2j\Delta N_m$ . Half of them belong to the self-hardened plane while the other half lie in the latent hardened planes. In an F.C.C. crystal, it is assumed that each of the three latent hardened planes contains  $j\Delta N_m / 3$  new links, i.e. on average  $j\Delta N_m / 3$  links are cut on each latent hardened plane.

$$\Delta N_{self} = j\Delta N_m \quad (12a)$$

$$\Delta N_{latent} = \frac{j\Delta N_m}{3} \quad (12b)$$

### 2.3.3.2 Multiple releases and expansion

Eq. (12) is effectively controlled by a single fitting parameter  $j$ . However, according to Foreman and Makin [25], each activated threshold link pre-held at weak obstacles of dislocation junctions has the possibility to significantly expand by coalescing with adjacent consecutively released links even shorter than the threshold links. As a result of these multiple releases, the link expands in an unzipping motion by simultaneously bypassing multiple pinning points until a new equilibrium condition is satisfied by the final network refinement process. The additional loss of links on the active slip plane associated with the multiple releases can be taken into account simply by introducing a scale factor  $\kappa$  ( $\kappa < 1$ ) into Eq. (12a)

$$\Delta N_{self} = (1 - \kappa) j \Delta N_m = j_s \Delta N_m \quad (13)$$

where  $j_s = (1 - \kappa) j$  is the combined parameter controlling the self-hardening, while the latent hardening is controlled only by  $j$  in Eq. (12b).

### 2.3.3.3 Evolution of the link length distribution

The pinning points on a single slip plane can originate from pre-existing junctions or newly formed junctions from cross-slip or the bowing of dislocations on other intersecting slip planes. The establishment of the link length distribution function in Eq. (8) has assumed a similarity between the number of links and the number of pinning points. Such a similarity is also used here, where the increase of the number of links on a slip plane is equal to the increase of the number of pinning points on the same plane. This avoids the consideration of the detailed origins of the pinning points on each slip plane, but retains the basic physics of the process. Note that the distribution function (Eq. (8)) is a unique function of the mean spacing or the number of pinning points  $N$ . Updating  $N$  using Eq. (12b) and Eq. (13) also updates the distribution function of pinning points as well as the link length distribution, but with different truncations at different threshold lengths during work hardening. Since self- and latent hardening are controlled by different parameters, the distribution functions on different slip planes may evolve in different ways.

## 3. Model evaluation

### 3.1. In situ neutron diffraction experiment

The material is Type 316H austenitic stainless steel supplied by EDF Energy. The three elastic constants  $C_{11}$ ,  $C_{12}$  and  $C_{44}$  of a single F.C.C. crystal of this stainless steel are listed in Table 1, with respect to the local co-ordinate system. The experimental data employed here was generated using the neutron diffraction (ND) technique, with measurements of the lattice response of Type 316H stainless steels obtained from experiments conducted on either the ENGIN-X instrument at ISIS, UK [2, 4, 5] or at Los Alamos National Laboratory, USA [1, 3, 28]. A detailed description of the experimental procedure can be found in [1-5, 28]. Figure 1(a) illustrates schematically the experimental setup. The changes in the lattice spacing of different crystallographic planes  $\{hkl\}$  measured during *in-situ* uniaxial tensile loading of the specimen at ambient temperature can be transformed to provide the evolution of elastic lattice strain. The average value within each oriented grain family was measured, such that the members in the family have planes with the same Miller indices  $\{hkl\}$  diffracting to the detector. Two detectors in the experiment guarantees a simultaneous collection of elastic lattice strains both parallel (axial) and perpendicular (radial) to the loading direction. The macroscopic strain of the bulk was measured by the extensometer attached to the specimen. An incremental loading history was used with alternative loading and unloading steps [1, 2, 4, 28]. Such a loading history ensured the measurement of both the elastic lattice strain during loading and residual elastic lattice strain after unloading. In this work, we focus on the data obtained from one typical grain family  $\{220\}$ .

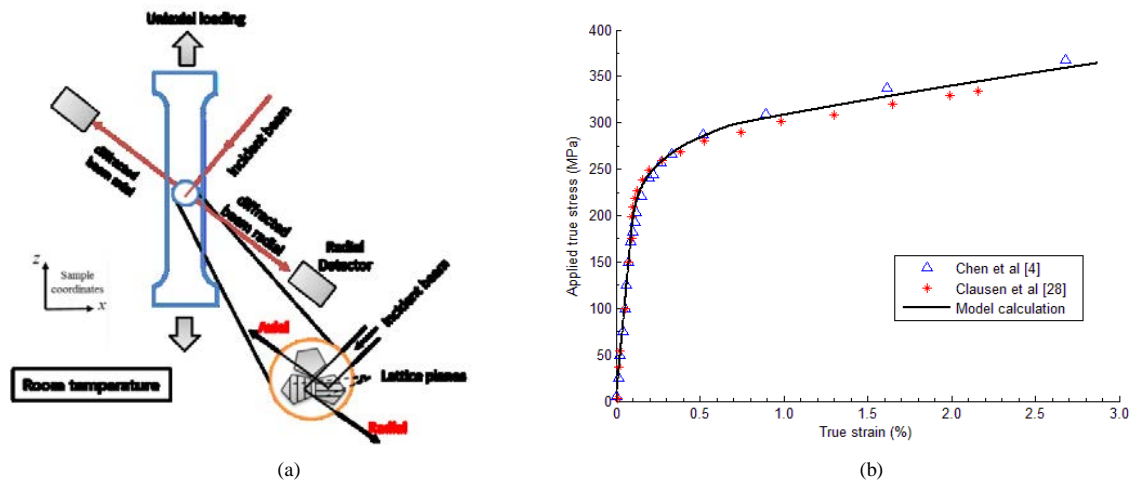


Fig. 1. (a) A schematic diagram of the neutron diffraction experiment setup, both axial and radial responses were collected; (b) Measured and simulated macroscopic polycrystal stress-strain response of 316H austenitic stainless steel under uniaxial tension at room temperature

### 3.2. Simulation procedure

In the simulations with the self-consistent model, the applied stress started from zero, with small but different increments employed during elastic and elasto-plastic deformation. The stress in each grain was then updated using Eq. (2a) and the plastic strain increment determined using Eq. (6). The macroscopic plastic strain increment for the polycrystal was then determined using the virtual work procedure described in section 2.1. The development of these incompatible plastic strains results in a change in the internal residual stress field. This was calculated using Eqs. (3) and (4), allowing the stress in each grain to be updated further with Eq. (5). This process was repeated until the maximum stress levels achieved in the experiments was reached. The values of the parameters used in the simulation are shown in Table 1. The only three fitting parameters were the initial number of pinning points on each slip plane ( $N_0$ ), the self-hardening factor ( $j_s$ ) and the latent hardening factor ( $j$ ). These parameters were chosen to provide the best fit to the experimental macroscopic stress-strain curve shown in Figure 1(b).

Table 1. Material parameters of Type 316H austenitic stainless steel used in the simulation

Parameter	Value	Parameter	Value
$C_{11}^a$	198 GPa	$p$	600
$C_{12}^a$	125 GPa	$\alpha$	0.35
$C_{44}^a$	122 GPa	$j_s$	1
$b$	$2.5 \times 10^{-10}$ m	$j$	5
$\Delta\gamma_0$	1	$N_0$	$6.5 \times 10^{13}$

<sup>a</sup>Data are taken from Kamaya [29]

### 3.3. Measurements and simulation results

Figure 2(a) compares the measured and predicted average results of the total lattice strain evolution for the {220} grain family along the axial direction (parallel to the  $z$ -axis in Figure 1(a)). Measurements from different researchers are also shown. Deviation from linearity indicates the occurrence of micro-yielding, which is discussed in detail in the next section. Figure 2(b) shows the evolution of the corresponding residual lattice strain, plotted against the macroscopic plastic strain for the bulk. Good agreement between the model prediction and the data was observed. The members of the {220} grain family have the {220} crystallographic plane normal to the loading axis. However,

the model predicts that all members experience the same strain along the loading direction and thus experience the same lattice strain during loading or residual lattice strain after unloading, i.e. there is no variation about the average. The measured results are therefore independent of which grains of this family are sampled in the experiments, which may explain the consistency of the ND measurements for this grain family obtained by different researchers.

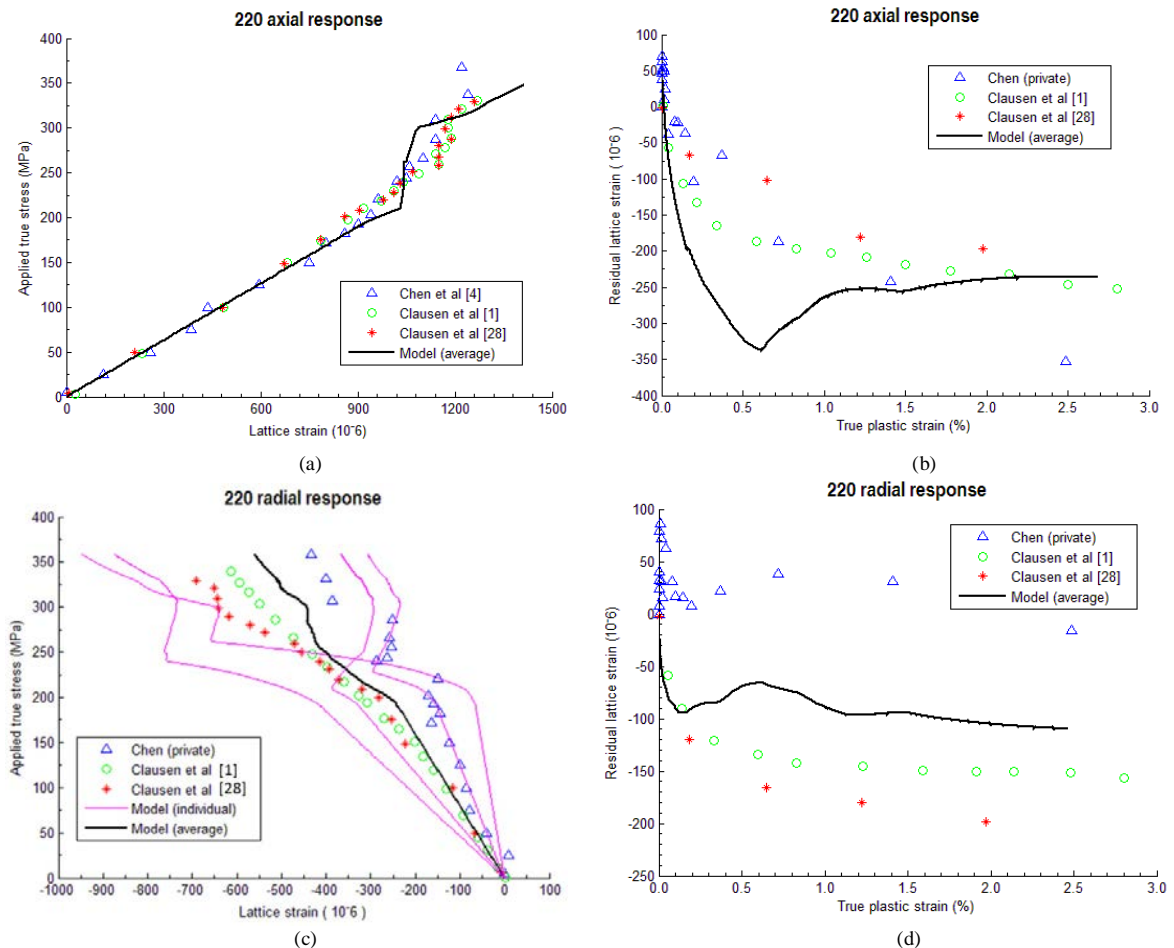


Fig. 2. Measured and predicted average results of the lattice strain evolution along (a) *axial* direction (*z*-axis in Fig. 1(a)) and (c) *radial* direction (*x*-axis in Fig. 1(a)) and the residual lattice strain evolution along (b) *axial* direction (*z*-axis in Fig. 1(a)) and (d) *radial* direction (*x*-axis in Fig. 1(a)) of {220} grain family. Data was measured by different researchers for the same grain family within the same materials.

The measured and predicted lattice response of the {220} grain family along the radial direction (*x*-axis in Figure 1(a)) are plotted in Figure 2(c) for the lattice strain evolution and Figure 2(d) for the residual lattice strain evolution. Again, the model prediction was compared with measurements from different researchers. In contrast to the axial response, the model now predicts a variation within the individual members of the {220} grain family in the radial direction. Responses from some members are presented in Figure 2(c). A relatively large scatter is also observed in the data. Although the averaged response captures the general trend and the result in individual members covers the full spread in the results, this figure demonstrates that measurements along the radial direction are less reproducible than that along the axial direction. This indicates that different experiments have sampled different combinations of members of the radial grain family. It is important to note that some grains which are members of the {220} grain family that diffract to the radial detector are not within the {220} grain family that diffract to the axial detector, thus the two detectors were sampling the responses of different groups of grains. Therefore, measurement on a “family of planes” is perhaps a more appropriate term than that associated with a “grain family”.

#### 4. Discussion

The intragranular residual stress associated with the development of incompatible plastic strains plays an important role in explaining the multiple forward and backward inflections in the lattice responses shown in Figure 2. Here we mainly discuss the axial response in Figures 2(a) & (b). Figure 2(a) shows a nonlinear response beyond an applied stress of approximately 200 MPa. Beyond this point there is a small decrease in slope compared to the initial elastic portion of the curve. This is due to the onset of micro-yielding in other grains of the polycrystal before the members of the family of {220} planes start to yield. Load is transferred from the plastically deforming grains to those that only deform elastically, resulting in a positive contribution to the lattice strain within the family of {220} planes from the resulting increase in residual stress (Eq. (4a)). This is also reflected in both the observed and predicted positive residual lattice strain in Figure 2(b) at very low levels of macroscopic plastic strain. The subsequent sharp increase in the slope observed in Figure 2(a) occurs because of the micro-yielding of the family of {220} planes. This results in these grains transferring stress to other grains, leading to a sharp reduction of the residual stress and related lattice strain (Figure 2(b)). The intragranular residual stress ceases change once the family of {220} planes experiences almost the same plastic strain increment as the polycrystal itself, see Figure 2(b). The plastic strains generated in the grains during each increment of loading are now compatible, i.e.  $\Delta\epsilon^{in}$  defined in Eq. (3) is zero, and the increase in elastic strain of the grains in the family of planes is given by the incremental form of Eq. (2), i.e. the subsequent relationship between the increments of lattice strain and stress is the same as that for an elastic material, and therefore the slope of the curve of Figure 2(a) asymptotes towards the initial slope. Understanding the development of mismatch, or residual stress, at the micro-scale, especially along the axial direction, is beneficial to the study of macroscopic phenomena such as the Bauschinger effect [30].

#### 5. Conclusion

In the present work, a detailed dislocation hardening mechanism and its effect on the micro-scale lattice response is investigated by a multi-scale self-consistent model for a polycrystalline material, which combines three different modelling approaches, i.e. continuum and crystal plasticity models and an improved dislocation link length model. The self-consistent scheme captures the interaction between slip planes (self- and latent hardening) and between each individual grain and the surrounding macroscopically isotropic polycrystalline matrix (mismatch). The model is used to evaluate and explain the neutron diffraction measurements (both along axial and radial directions) of the lattice response of a typical family of {220} planes within an F.C.C. Type 316H polycrystalline austenitic stainless steel subjected to uniaxial tensile loading at ambient temperature. The consistency and scatter of data measured by different researchers is explained.

In particular, the model demonstrates that the axial response is stable and experimentally reproducible while there is significant scatter in the radial response. Neutron diffraction measures the lattice response of different families of grains at the axial and radial detectors. The stress is the same in all grain members that contribute to the measurement at the axial detector, but there are significant differences in the responses of the individual grains sampled by the radial detector; thus the data generated at the radial detector is sensitive to the detailed orientations of the grains that make up the family of planes that are sampled by the detector. The mismatch of intragranular residual stress plays an important role in explaining the nonlinear behaviour observed after micro-yielding. The model described here can be applied to other polycrystalline materials and it can be extended to include other contributions to yield and material hardening, like solute elements and precipitates [31].

#### Acknowledgements

The authors are grateful to the EDF Energy for supplying the material and supporting the research described in this paper. We also acknowledge the ISIS facility for the provision of neutron beamtime at the ENGIN-X beamline at the Rutherford Appleton Laboratory.

## References

- [1] Clausen B, Lorentzen T, Leffers T. Self-consistent modelling of the plastic deformation of FCC polycrystals and its implications for diffraction measurements of internal stresses. *Acta Mater* 1998;46:3087-98.
- [2] Daymond MR, Bouchard PJ. Elastoplastic deformation of 316 stainless steel under tensile loading at elevated temperatures. *Metall Mater Trans A* 2006;37A:1863-73.
- [3] Neil CJ, Wollmershauser JA, Clausen B, Tome CN, Agnew SR. Modeling lattice strain evolution at finite strains and experimental verification for copper and stainless steel using in situ neutron diffraction. *Int J Plasticity* 2010;26:1772-91.
- [4] Chen B, Hu JN, Flewitt PEJ, Smith DJ, Cocks ACF, Zhang SY. Quantifying internal stress and internal resistance associated with thermal ageing and creep in a polycrystalline material. *Acta Mater* 2014;67:207-19.
- [5] Li DF, O'Dowd NP. On the evolution of lattice deformation in austenitic stainless steels-The role of work hardening at finite strains. *J Mech Phys Solids* 2011;59:2421-41.
- [6] Hu JN, Chen B, Smith DJ, Flewitt PEJ, Cocks ACF. A self-consistent model in the local residual stress evaluation of 316H stainless steel. 13th International Conference on Fracture, Beijing 2013.
- [7] Lagneborg R, Forsen BH. A model based on dislocation distributions for work-hardening and the density of mobile and immobile dislocations during plastic flow. *Acta Metall Mater* 1973;21:781-90.
- [8] Ostrom P, Lagneborg R. A recovery-athermal glide creep model. *J Eng Mater-T Asme* 1976;98:114-24.
- [9] Eshelby JD. The determination of the elastic field of an ellipsoidal inclusion and related problems. *Proc R Soc Lond A* 1957;241:376-96.
- [10] Mura T. *Micromechanics of defects in solids*. The Hague ; London: Martinus Nijhoff; 1982.
- [11] Kroner E. On the Plastic Deformation of Polycrystals. *Acta Metall Mater* 1961;9:155-61.
- [12] Budiansky B, Wu TT. Theoretical prediction of plastic strains of polycrystals. *Proc 4th Congr Appl Mech* 1962:1175-85.
- [13] Hu JN. A theoretical study of creep deformation mechanisms of Type 316H stainless steel at elevated temperatures. DPhil Thesis, University of Oxford, To be submitted 2014.
- [14] Asaro RJ, Needleman A. Overview .42. Texture Development and Strain-Hardening in Rate Dependent Polycrystals. *Acta Metall Mater* 1985;33:923-53.
- [15] Kocks UF, Mecking H. Physics and phenomenology of strain hardening: the FCC case. . *Progress in Materials Science* 2003;48:171-273.
- [16] Hutchinson JW. Bounds and Self-Consistent Estimates for Creep of Polycrystalline Materials. *Proc R Soc Lon Ser-A* 1976;348:101-27.
- [17] Bronkhorst CA, Kalidindi SR, Anand L. Polycrystalline Plasticity and the Evolution of Crystallographic Texture in Fcc Metals. *Philos T Roy Soc A* 1992;341:443-77.
- [18] Ajaja O. A Dislocation Network Model of Recovery-Controlled Creep. *J Mater Sci* 1986;21:3351-6.
- [19] Shi L, Northwood DO. On Dislocation Link Length Statistics for Plastic-Deformation of Crystals. *Phys Status Solidi A* 1993;137:75-85.
- [20] Ardell AJ, Przystupa MA. Dislocation Link-Length Statistics and Elevated-Temperature Deformation of Crystals. *Mech Mater* 1984;3:319-32.
- [21] Ardell AJ, Lee SS. A Dislocation Network Theory of Harper-Dorn Creep .1. Steady-State Creep of Monocrystalline Al. *Acta Metall Mater* 1986;34:2411-23.
- [22] Lin P, Lee SS, Ardell AJ. Scaling Characteristics of Dislocation Link Length Distributions Generated during the Creep of Crystals. *Acta Metall Mater* 1989;37:739-48.
- [23] Lagneborg R. Recovery Creep in Materials Hardened by a Second Phase. *J Mater Sci* 1968;3:596-602.
- [24] Lagneborg R. A modified recovery-creep model and its evaluation. *Metal Science* 1972;6:127-33.
- [25] Foreman AJE, Makin MJ. Dislocation Movement through Random Arrays of Obstacles. *Philosophical Magazine* 1966;14:911-24.
- [26] Friedel J. *Dislocations*. Reprinted with corrections ed. Oxford, Reading, Mass: Pergamon; [Distributed in USA by] Addison-Wesley Pub. Co; 1964.
- [27] Madec R, Devincere B, Kubin LP. From dislocation junctions to forest hardening. *Phys Rev Lett* 2002;89.
- [28] Clausen B, Lorentzen T, Bourke MAM, Daymond MR. Lattice strain evolution during uniaxial tensile loading of stainless steel. *Mat Sci Eng a-Struct* 1999;259:17-24.
- [29] Kamaya M. A procedure for estimating Young's modulus of textured polycrystalline materials. *Int J Solids Struct* 2009;46:2642-9.
- [30] Pedersen OB, Brown LM, Stobbs WM. The Bauschinger Effect in Copper. *Acta Metall Mater* 1981;29:1843-50.
- [31] Dong Y, Nogaret T, Curtin WA. Scaling of Dislocation Strengthening by Multiple Obstacle Types. *Metall Mater Trans A* 2010;41A:1954-60.